Eur. Phys. J. E **17**, 93–100 (2005)
DOI 10.1140/epje/i2005-10002-2

THE EUROPEAN PHYSICAL JOURNAL E

From the stress response function (back) to the sand pile "dip"

A.P.F. Atman[1,a], P. Brunet[1,b], J. Geng[2], G. Reydellet[1], P. Claudin[1,c], R.P. Behringer[2], and E. Clément[1]

[1] Laboratoire de Physique et Mécanique des Milieux Hétérogènes, ESPCI, 10 rue Vauquelin, 75231 Paris Cedex 05, France[d]
[2] Department of Physics & Center for Nonlinear and Complex Systems, Duke University, Durham NC, 27708-0305, USA

Received 6 January 2005 /
Published online: 6 April 2005 –

Abstract. We relate the pressure "dip" observed at the bottom of a sand pile prepared by successive avalanches to the stress profile obtained on sheared granular layers in response to a localized vertical overload. We show that, within a simple anisotropic elastic analysis, the skewness and the tilt of the response profile caused by shearing provide a qualitative agreement with the sand pile dip effect. We conclude that the texture anisotropy produced by the avalanches is in essence similar to that induced by a simple shearing —albeit tilted by the angle of repose of the pile. This work also shows that this response function technique could be very well adapted to probe the texture of static granular packing.

PACS. 45.70.-n Granular systems – 45.70.Cc Static sandpiles; granular compaction – 46.25.-y Static elasticity

The stress distribution below a pile of sand has been one of the problematic issues of the statics of granular materials in physics over the last few years [1]. In fact, experiments have shown that, when a granular pile is prepared from a point source, the bottom pressure profile has a clear local minimum —a "dip"— below the apex [2–4]. The existence of this pressure dip has been strongly debated, and it is now well established that the presence or absence of this dip is closely related to the preparation history of the pile. This was demonstrated by Vanel *et al.* [4]. Using the same sand and experimental apparatus, these authors could generate the stress dip using a localized deposition technique or cause the dip to disappear by constructing a pile in successive horizontal layers. Similar conclusions were reached for two-dimensional heaps with photo-elastic grains [5], and in numerical simulations [6–8].

This interesting effect has inspired the development of new models to describe how forces are transmitted in dense granular materials. Among them are those proposed by Bouchaud *et al.*, initially developed in the context of the sand pile dip [9–12], and further extended to other geometries like that of the silo [12,13]. This approach is also intended to describe a collection of systems including dense colloids, granular matter or foams [14]. At the macroscopic level, these features are modelled by hyperbolic, partial differential equations (PDE) for the stress tensor. Although no explicit link was established, the characteristics of these hyperbolic equations were intuitively thought to be related to the mesoscopic "force chain" network whose structure and orientation were shaped by the previous history of the granular assembly —see also [15, 16] concerning force chains. Plasticity theories for granular deformations are also of hyperbolic type, although conceptually different than the previous cited models. From the classical, soil mechanics point of view, below the plastic threshold, granular material is thought to behave as an effective elastic material with PDEs that belong to the elliptic class [17]. Finally, sound wave propagation techniques and numerical simulations of confined granular assemblies indicate that that assessment of effective elastic constitutive relations is still an open and difficult issue [18].

In order to distinguish between the very different mathematics of hyperbolic and elliptic PDEs, a stress response experiment was proposed [9,19]. For instance, the pressure profile measured at the bottom of an isotropic elastic horizontal layer in response to a localized vertical overload at its top surface should be a single broad peak, while hyperbolic models would yield in 2D two thin peaks or a ring in 3D. Several experiments [20–26] and simulations [27–36] have recently addressed the issue of the stress response in a granular layer. Collectively, they have demonstrated two key points:

i) the shape of the pressure response profiles is generally not in agreement with the predictions of the hyperbolic

[a] *Present address*: Departamento de Física, Instituto de Ciências Exatas, Universidade Federal de Minas Gerais, C.P. 702, 30123-970, Belo Horizonte, MG, Brazil.
[b] *Present address*: Royal Institute of Technology, Department of Mechanics, 10044 Stockholm, Sweden.
[c] e-mail: `claudin@ccr.jussieu.fr`
[d] The LPMMH is UMR 7636 of the CNRS.

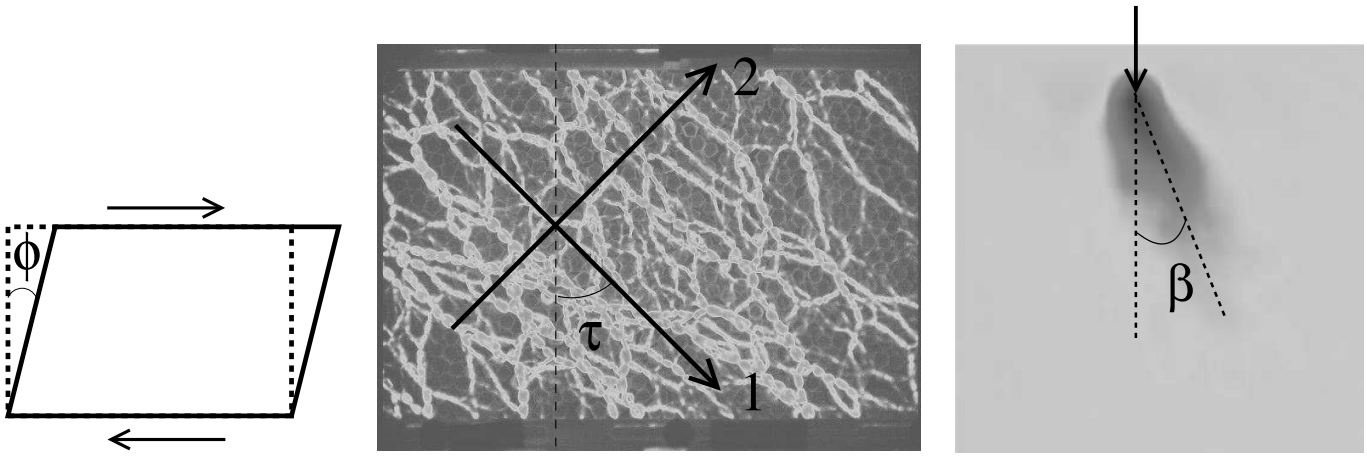

Fig. 1. Left: sketch of the 2D shear box. The system is strained up to an angle ϕ. Middle: visualization of the force chains after shearing. The analysis of their orientations shows that a direction at $\tau = 45^\circ$ is preferred [25]. Right: average response to a vertical overload after shearing with a strain angle $\phi = 5^\circ$. The stress maximum is oriented at $\beta = 22^\circ$ to the vertical.

models. For the generic case of a disordered packing of frictional grains, the measured profiles show an elliptic-like behavior with one single peak broadening in proportion to the thickness/depth of the layer — except in [20]. For well-ordered packing, the measured response functions may produce rays diverging from the source, but this type of response is also compatible with anisotropic elasticity [30,37,38];

ii) the geometry of the response function is in fact simpler than that of the pile, and offers rich possibilities. Response function measurements directly detect any symmetry breaking due to texture originating from either a specific preparation or from any other external action on the pile. The layer can be loose, dense, compacted, sheared, avalanched, sedimented, ordered, vibrated, and so on.

Nevertheless, there are still a number of unresolved questions. For instance, in the limiting case of isostatic pilings, numerical simulations [39,40] and theoretical arguments [41–44,16] indicate that hyperbolic equations should describe the stress propagation, although this is not in agreement with the work of Roux [45].

Experiments have shown that the response to a point force is very sensitive to the preparation of the system [34]. For instance, for a 2D system which has been subjected to strain in a 2D shear box, the response function is skewed in the direction of the shear [25] showing a strain-induced anisotropy. Here, we extend this result to 3D granular assemblies and propose a relation to the pressure "dip" observed at the bottom of a sand pile when prepared by successive avalanches. Interestingly, anisotropy induced by preparation was suggested by Savage [46] to explain this phenomenon. Note that the occurrence of a stress solution with a dip can also be produced in a model pile composed of an elastic core and plastic wings [47].

The paper is organized as follows. We first describe experimental results obtained for the response of a sheared granular layer in 2D and in 3D (Sect. 1) and for a layer prepared by successive avalanches. We then present a theoretical anisotropic elastic analysis of these experimental data in 2D and a numerical analysis in 3D (Sect. 2). Thereafter, we numerically solve the case of a conical heap (Sect. 3). We close with conclusions and suggested perspectives.

1 Experimental response function on sheared granular layers

The response function experiments of interest here, were carried out in shear cell geometries in two and three dimensions. In both cases, the cell consisted of vertical boundaries that could be tilted quasi-statically by an angle ϕ with respect to the vertical axis. This process deformed the samples from an original rectangular geometry to that of a parallelogram.

In 2D, the spacing between the horizontal boundaries was maintained strictly constant, so that the sample volume also remained constant. The particles were pentagons made of a photo-elastic material, which allows a direct measurement of the local force response and of the force chains. More details on these experiments can be found in Geng *et al.* [25]. As we can see from Figure 1, the salient features of these series of experiments are i) the force chain network is oriented at 45° from the horizontal axis, which is the principal compressive direction, and ii) the response to a vertical force is tilted with an angle β with respect of the vertical direction, which illustrates perfectly the symmetry breaking due to shearing. In a previous contribution we argue that this $\tau = 45^\circ$ angle is simply related to the principal axes of compression and dilation (respectively, directions 1 and 2 in Fig. 1).

In 3D, we carry out two experiments to extend the study of the influence of shear on the texture of a granular assembly. First, we built an apparatus similar to the shear cell already used in 2D. Second, we deposited the material in a horizontal layer by the superposition of successive avalanches.

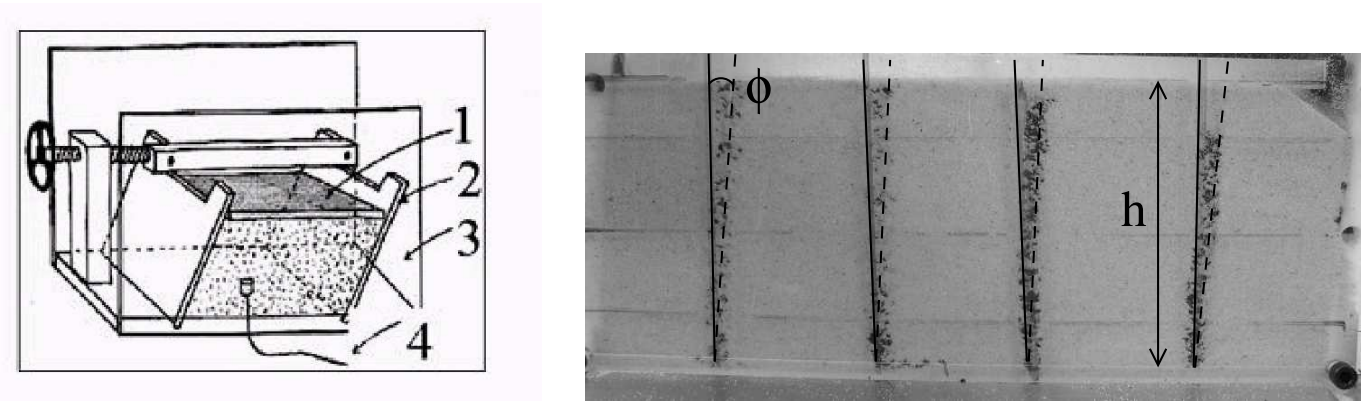

Fig. 2. Left: sketch of the 3D shear box. 1 top lid, 2 tiltable lateral boundaries, 3 fix glass wall, 4 capacitive stress probe. Right: visualization of the grain displacement due to shear. Coloured grains have been put along four vertical lines before shearing. These grains are located along inclined lines afterwards, so that the strain field of the layer looks reasonably homogeneous.

The shear cell

The shear cell is sketched in the left part of Figure 2. In order to probe the mechanical properties and the symmetries associated with the induced structure, we mounted a capacitive stress probe at the bottom of the cell (labeled 4 in Fig. 2); the applied force on the top (labeled 1) is moved horizontally. Specifically, the force response measurements use a low-frequency modulation of the localized stress imposed at the top of the sample, and lock-in detection of the vertical pressure response on the bottom, as described by Reydellet *et al.* [21]. The lock-in detection provided a large signal/noise ratio, which allowed us to apply tiny forces, of the same order as the weight of few grains. This prevented any significant deformation of the packing which would have modified the fragile structure of contacts. A horizontal layer of grains (Fontainebleau sand, slightly polydisperse round grains, $d \sim 300$ μm size) was initially prepared by pouring the material into shear box of horizontal size $l = 25$ cm. The lateral width of the box was $w = 20$ cm. The total height h of sand ranged between 4 and 15 cm.

The pouring procedure involved a sieve which was slowly raised in order to create a uniform rain of sand. Thereafter the sand layer was packed by pushing on the free surface with a plate, and by simultaneously taping on the lateral edges of the box. Note that these conditions are similar to the so-called "dense preparation method" proposed earlier by Serero *et al.* [22]. A vertical stress response was determined before and after shearing. During the shear deformation of the sample, a weight (~ 40 kg) was imposed on the top surface and the lateral boundaries (labeled as 2 on the left of Fig. 2) were slowly tilted up to a final angle ϕ. The dense preparation as well as the large imposed load seemed necessary to avoid inhomogeneous deformations of the free surface and help to hinder the formation of localized shear bands. This result was confirmed by direct inspection of the displacement fields of the grains lying on the transparent side of the lateral boundaries. In order to monitor this displacement field, three vertical columns of coloured grains were inserted next to the lateral boundaries prior to shearing (see the right panel of Fig. 2). We note that the formation of a shear band was hindered only for limited values of aspect ratios (typically for ratios h/l from 0.3 to 1 used here) and for shear angles smaller than 5°. We also point out that due to the rather close-to-unit aspect ratio of the shear box, the response for large horizontal distances between the source and the stress probe was not measured so as to avoid the influence of lateral walls.

In Figure 3, we show the experimental results for the vertical stress response σ_{zz} after shear for several shear angles ϕ and layer depths h. In this figure, the abscisa is

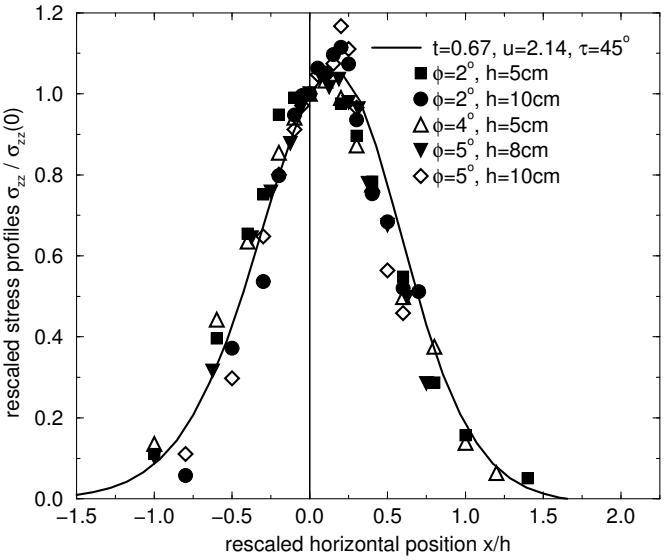

Fig. 3. Response profiles of a 3D sheared layer of Fontainebleau sand for various values of the layer thickness h and the strain angle ϕ. The maxima of the profiles correspond to a tilt angle β of $8° \pm 1°$. The collapse of the data is reasonably fitted by the SEM (see Sect. 2 for the definition of the SEM and the choice of the different parameters, *e.g.* Poisson ratios, etc.) with $t = 0.67$ and $u = 2.14$ when τ is set to 45°.

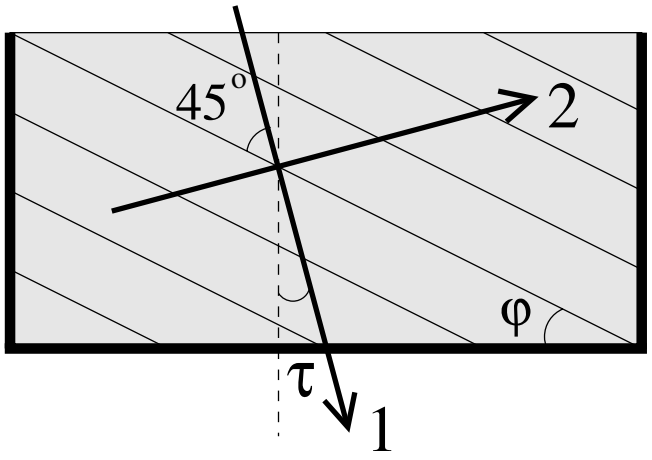

Fig. 4. Sketch of the avalanche preparation procedure. The avalanche angle is $\varphi = 30°$, so that the expected angle of anisotropy is $\tau = 15°$.

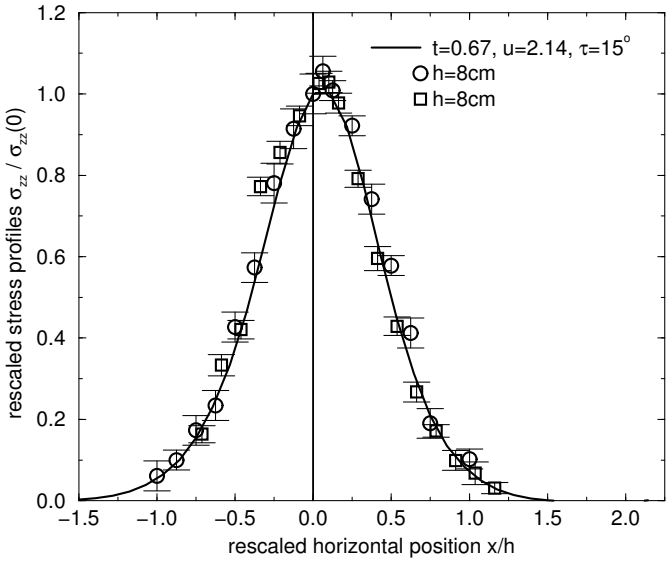

Fig. 5. Two response profiles of a 3D layer of Fontainebleau sand prepared by successive avalanches. The thickness of the layer is $h = 8$ cm. In comparison to Figure 3, the shape of the profile is also well reproduced by the SEM (again, see Sect. 2) with $t = 0.67$ and $u = 2.14$ but now when τ is set to 15°.

the horizontal coordinate x normalized by the sand depth h. We normalize the stresses $\sigma_{zz}(x)$ by $\sigma_{zz}(0)$, the value of the stress at $x = 0$ (*i.e.* immediately below the piston). This normalization is due to the finite lateral extension of the box since, contrary to previous situations [21,22], we cannot obtain a proper normalization of the stress by integration (*i.e.* assess the total force applied). For shear angles ϕ varying from 2° to 5°, the experiments clearly show a skewing of the response function in association with a displacement of the maximum corresponding to an angle $\beta = 8° \pm 1°$ (deduced from the slope of the empirical relation between the height of sand and the shift). Thus, as in the 2D case, the response indicates that, due to shearing, the granular assembly is clearly anisotropic (at least, the vertical direction is no longer an axis of symmetry). It is worth mentioning that this tendency is robust, as it was observed for other types of grains (larger, slightly polydisperse, rough sand grains of diameter ~ 1 mm, and smooth spherical beads of diameter ~ 1.5 mm).

The avalanche preparation

Next we prepared a layer of sand structured by successive avalanches (see Fig. 4 for a sketch of the preparation procedure). The experimental results for two independent preparations are displayed in Figure 5 and rescaled in a way similar to the case of the 3D shear box. Again, we observe a skewing of the response indicating an anisotropic texture induced by the avalanches. However, the tilt effect of the response is weaker, as it corresponds to an angle for the locus of the maxima $\beta = 3.5° \pm 1°$.

2 Elastic calculations

We next turn to modeling the experimental results using elasticity theory. We show here that a simple anisotropic description is sufficient to capture all the salient features of the data. Isotropic elasticity, in both 2D and 3D, has only two constitutive parameters for a given material, namely the Young modulus E and the Poisson ratio ν. When anisotropy is introduced, however, the number of independent parameters increases significantly. For example, five parameters are required for the case of simple 2D orthotropy that we use below. In 3D, this number is even higher. Fortunately, for the static equations, only combinations of these parameters enter (*e.g.* the parameters r and t, below). Still, a meaningful fit of the response profiles to an anisotropic elastic model is a formidable task. Although such an approach is very instructive, it is not an essential point for the present purposes. We will present the results of this type of approach elsewhere.

2.1 Elastic response in 2D

Let us first focus on the simpler two-dimensional case. What is indicated by the 2D shearing experiment described in the previous section, is that the sheared force chain network clearly has a preferred direction at an angle of 45° with respect to the initial axis of the box. Contacts between the grains are gained or reinforced in this strong direction, whereas they are lost or weakened in the perpendicular direction. It is then expected that an effective elastic medium model for this situation would have a stiff direction (direction 1) which makes a fixed angle $\tau = 45°$ relative to the vertical axis z (x denotes the horizontal coordinate) characterized by a Young modulus E_1. Perpendicularly to direction 1 is the softer direction (direction 2) that is characterized by a Young modulus $E_2 < E_1$. This orthotropic elastic description is completed by three additional parameters: two Poisson coefficients ν_{12} and ν_{21} and the shear modulus G. Then, the strain-stress relation,

expressed in these tilted axis, can be written in the following matrix form:

$$\begin{pmatrix} u_{11} \\ u_{22} \\ u_{12} \end{pmatrix} = \begin{pmatrix} \frac{1}{E_1} & -\frac{\nu_{21}}{E_2} & 0 \\ -\frac{\nu_{12}}{E_1} & \frac{1}{E_2} & 0 \\ 0 & 0 & \frac{1}{2G} \end{pmatrix} \begin{pmatrix} \sigma_{11} \\ \sigma_{22} \\ \sigma_{12} \end{pmatrix}, \quad (1)$$

Because the matrix involved in this relation must be symmetric, the Young moduli and Poisson ratios are not independent, but satisfy the relation $E_2/E_1 = \nu_{21}/\nu_{12}$. The elastic free energy is well defined if

$$E_1, E_2, G > 0, \quad (2)$$

$$1 - \nu_{12}\nu_{21} > 0. \quad (3)$$

The isotropic case is recovered for $E_1 = E_2 = E$, $\nu_{12} = \nu_{21} = \nu$ and $G = \frac{E}{2(1+\nu)}$.

In reference [38], Otto *et al.* have analytically computed the stress tensor components for such an anisotropic elastic material in the case of a semi-infinite medium ($z > 0$) loaded with a unitary point force at the origin $x = z = 0$. They have shown that, for a given anisotropy angle τ, the stress response profiles only depend on two quantities that involve a combination of the elastic coefficients:

$$t = E_2/E_1 = \nu_{21}/\nu_{12}, \quad (4)$$

$$r = \frac{1}{2} E_2 \left(\frac{1}{G} - \frac{\nu_{12}}{E_1} - \frac{\nu_{21}}{E_2} \right). \quad (5)$$

It is notable that for other geometries, the stresses could depend on the E's, ν's or G independently of t and r due to the effect of different boundary conditions, for example at the bottom of a finite thickness slab. By contrast, the corresponding familiar isotropic solution is completely independent of E and ν, although some (weak) variations of the stress profiles with ν are found for an isotropic layer of finite thickness [22,48]. Depending on the values of τ, and in particular on the sign of r, and of $(r^2 - t)$, different response shapes result, including single- or double-peaked responses, and symmetrical or skewed profiles (see numerous figures in [38]).

Although it is natural to fix the angle τ and to use the ratio E_2/E_1 as a control parameter for the amplitude of the anisotropy created by the shearing, it is rather difficult to have any kind of intuition about the ν's and the shear modulus G, *i.e.* on r. Figure 6 shows the locus of values of r and t which give a response profile for a semi-infinite medium with a deflection angle of $\beta = 22°$, the experimental value. Interestingly, we see the tendency for a higher value of r to significantly broaden the response function. This would correspond, for example, to small values of the shear modulus G. Note also, that the width at half-height of the response is a quantity that is easily accessible experimentally, and hence provides a good method to test this type of model.

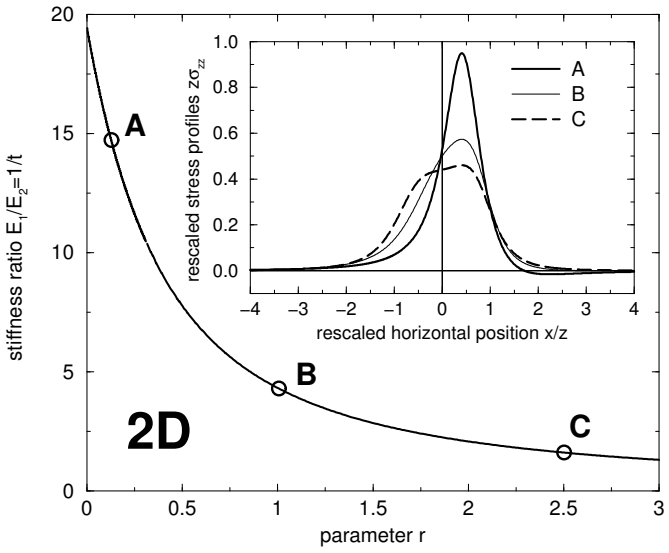

Fig. 6. Values of r and t which give a response profile for a semi-infinite medium with a tilt angle of $\beta = 22°$. Inset: three particular such stress profiles: $r = 0.15$ and $t = 0.07$ (A, bold line), $r = 1.0$ and $t = 0.24$ (B, thin line), and $r = 2.5$ and $t = 0.62$ (C, dashed line). The response shape is wider for larger r.

2.2 Elastic response in 3D

It is not difficult to generalize this approach to 3D. However, in this case, two axes (directions 2 and 3) orthogonal to direction 1 must be specified. We keep the notation x for the horizontal axis along which the shearing is applied, and the stress response measured. Direction 2 is in the vertical plane (z, x), and direction 3 (y) is perpendicular to these two directions.

The matrix involved in the 3D equivalent of the strain-stress relations (1) has a similar structure to the 2D case, but with three Young moduli E_i, three shear moduli G_i and six Poisson ratios ν_{ij} (i and j must be different). Again, the symmetry of the matrix gives three relations of the form $\nu_{ij}/E_i = \nu_{ji}/E_j$. In the final analysis, there are 9 independent coefficients besides the anisotropy angle τ. Stability now requires that

$$E_i, G_i > 0, \quad (6)$$

$$1 - \nu_{ij}\nu_{ji} > 0, \quad (7)$$

$$1 - \sum_{i \neq j} \nu_{ij}\nu_{ji} - \nu_{12}\nu_{23}\nu_{31} - \nu_{21}\nu_{32}\nu_{13} > 0. \quad (8)$$

Unfortunately, in 3D, we do not yet have closed-form analytic expressions for the stress response profiles comparable to those given in [38]. To compute profiles in 3D, we make use of a finite element free-ware code developed in soil mechanics called CASTEM [49]. We typically chose a grid with $40 \times 40 \times 12$ cells in the x-, y- and z-direction, respectively. In this section, we show that the trends suggested by the experimental data are reproduced rather well in a model that allows for a modification of the constitutive elastic relations with respect to the symmetry of the external deformation applied to the system.

Here, we analyze the previous 3D experiments on the shear box and on the avalanche preparation. We

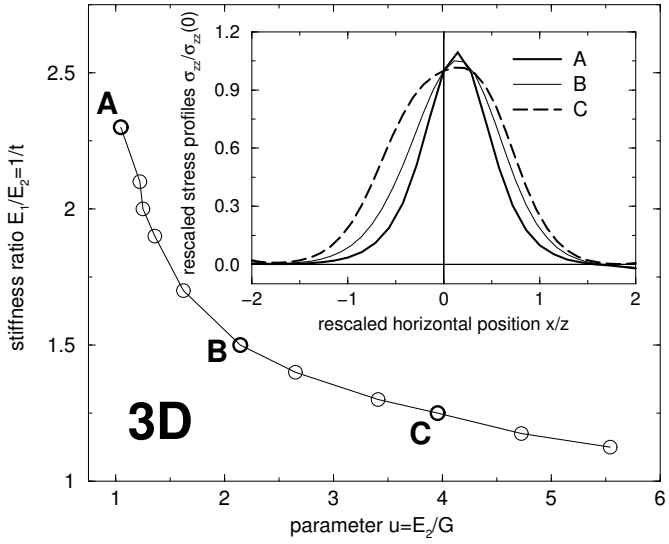

Fig. 7. 3D equivalent of Figure 6: values of u and t which give a response profile with a tilt angle of $\beta = 8°$. Note, however, that these 3D calculations have been performed numerically with CASTEM on a layer of *finite* thickness. Inset: three particular such stress profiles: $u = 1.05$ and $t = 0.43$ (A, bold line), $u = 2.14$ and $t = 0.67$ (B, thin line), and $u = 3.96$ and $t = 0.8$ (C, dashed line). The response shape is wider for larger u.

emphasize that we do not make a detailed fit of the experimental data to a general anisotropic elasticity model. Using the numerical code, we only explore the possibilities of orthotropic elasticity on a "Simple Elastic Model" that we call SEM in the sequel. Again, we do not seek a complete exploration of the parameter space and thus, we only vary three parameters that we believe are crucial, namely, the stiffness of the direction of anisotropy E_1, the shear modulus G and τ the direction of the orthotropic axis with respect to the vertical direction. More precisely, we consider the same value of G for all directions, *i.e.* $G_1 = G_2 = G_3 = G$. The average Young modulus is taken constant: $E = (E_1 + E_2 + E_3)/3 = 150$ MPa. We also take $E_2 = E_3$. Finally, the three Poisson coefficients ν_{12}, ν_{13} and ν_{23} are also kept constant and bear the values $\nu = 0.3$. We checked that the value of this parameter is not very sensitive. The remaining ν_{ij} are such that the strain-stress matrix is symmetrical (see above). In the spirit of the 2D analytical results, we use two-dimensionless parameters to present our data, *i.e.* the stiffness ratio $t = E_2/E_1$, and the shear ratio $u = E_2/G$. u is analogous to the parameter r in 2D —see equation (5).

The shear cell

An essential result of the shear box experiment was that the tilt angle of the stress response profiles is around 8° (Fig. 3). As suggested in the 2D space, it is natural that the orthotropic direction is tilted with an angle $\tau = 45°$. In Figure 7 we thus present the curve $t(u)$ corresponding to a tilt angle $\beta = 8°$ and for $\tau = 45°$ as computed by CASTEM using the SEM. We see that similarly to the 2D situation, moving on this curve from lower to higher values of u significantly enlarges the width of the response function (see the inset of Fig. 7). This is indeed an experimental observable that can be used to discriminate in parameter space. In the framework of the SEM, good agreement with the experimental data on the shear box can be obtained for values $u_0 = 2.14$ and $t_0 = 0.67$. The curve corresponding to (u_0, t_0) is presented in Figure 3.

The avalanche preparation

Now, we seek an interpretation of the response function for the granular slab prepared by successive avalanches. First we note that during the avalanching process, the flowing layer experiences a strong shear along the avalanche angle φ. An interesting outcome of the shear box experiment is that for all finite shear angle values ϕ that we tested, the shape of the response function as well as tilt angle β did not vary significantly. We argue that each deposited layer retains a memory of the shear due to the avalanching process, which induces an anisotropic texture. In first approximation, we may assume that the avalanche acts like a shear box whose bottom is tilted at an angle $\varphi \sim 30°$ with respect to the horizontal direction. We propose to use the parameters (u_0, t_0) which compare reasonably to the shear box data to interpretate the avalanche deposition experiment. Of course, now, we need to tilt the orthotropic angle τ from 45° to a value $\tau = 45° - \varphi \sim 15°$. In Figure 5 we present the results of CASTEM calculations on the SEM using these parameters and indeed we find an angle $\beta = 3.0° \pm 0.5°$, close to the experimental value $\beta = 3.5° \pm 1°$.

3 Back to the sand pile pressure profile

Several experimental determinations of the stress distribution below a sand pile prepared from a point source were obtained under various experimental conditions. First, we note that all stress data can be rescaled so that it is possible to compare the prediction of the elastic model with experiments made with different pile sizes. For a conical pile of height h, radius at the base $R = h/\tan\varphi$, and pile slope angle φ, the relevant parameters are the rescaled vertical stress $\sigma_{zz}/\rho g h$ and the rescaled horizontal position $\xi = r/R$ (ρ is the density of the granular packing and g the gravity constant).

In Figure 8, we show the experimental data obtained by three groups, Šmíd and Novosad [2], Brockbank *et al.* [3] and Vanel *et al.* [4]. The underlying idea behind the use of an anisotropic elasticity is to include the frozen texture caused by shearing that ensues during avalanche deposition. From the response function experiments under shearing (shear box and avalanche) displayed before, it is natural to propose a modelling of the sand pile prepared by successive avalanche using an orthotropic elastic model like SEM. Of course, we see here the limitations of such a modelling, since in the SEM version of the CASTEM

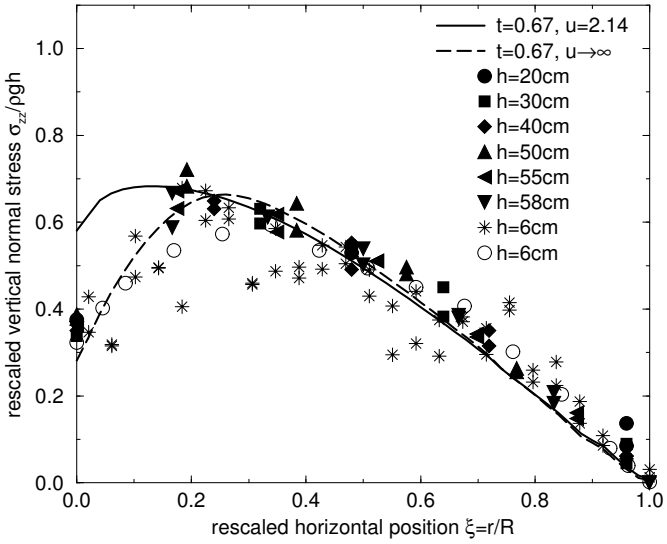

Fig. 8. Normal stress below a conical pile. Filled symbols are the data of Šmíd and Novosad [2], the stars are from Brockbank *et al.* [3], and the empty circles show Vanel *et al.*'s measurements [4]. The corresponding pile heights h are indicated in legend. The repose angles of the material used by these authors are, respectively, $\varphi = 33°$, $\varphi = 31°$ and $\varphi = 30°$. For simplicity, we have set $\varphi = 30°$ in all our calculations. The solid line is the prediction of the SEM in the conical geometry with $t = 0.67$ and $u = 2.14$ when τ is set to 15°. The dashed line is the same except for $u \to \infty$, which seems to fit better the data.

computation we only have three parameters to vary. Furthermore, as discussed previously, in the case where the sand pile repose angle is $\varphi = 30°$, the orthotropic direction should be fixed at $\tau = 15°$. We show in Figure 8 the results of a CASTEM computation for a conical sand pile using the "optimal" parameters (u_0, t_0) that yielded a reasonable agreement to the shear box and the avalanche deposition experiments. Note that we also checked that the stress state is always below the Coulomb criterion (with an internal friction angle of 30°), *i.e.* that failure never occurs —except marginally at the very free surface as all stress components vanish.

We observe the presence of a dip that bears essentially the correct qualitative features. Nevertheless, on a quantitative level, the values of the depth of the dip as well as the amplitude of the stress maximum seem too large. Furthermore, the value of $\xi_{\max} \sim 0.15$ underestimates clearly the experimental data. In fact the data seem to be better fitted by the SEM with a very small shear modulus, *i.e.* $u \to \infty$. The understanding of this observation remains an open question.

4 Conclusion

In this paper we present an analysis of several response function experiments under the scope of anisotropic elasticity. As an application, we investigate to which extent the pressure dip observed at the bottom of a sand pile prepared by successive avalanches can be understood as a texturing effect induced by shearing along the avalanche directions.

In the context of an elastic analysis, the orthotropic model used in this paper is relatively simple, since its main features are the presence of a stiff axis in the orthotropic direction and a shear modulus that can be varied independently. The orthotropy axis direction is a third parameter simply taken at an angle $\pi/4$ with respect to the shearing direction. This choice corresponds to the direction of principal compression and is consistent with our recent experimental findings in 2D [25]. We also present new sets of experiments on a 3D sand packing in a shear box, where shear-induced anisotropy is present. The second experiment is a sheared granular slab constructed by successive avalanches. The agreement with the orthotropic model is quantitatively correct, as the tilt of the response function can be reproduced by elastic modelling in both experiments using the same set of parameters.

In a second series of analysis, we use the best fit parameters obtained from comparison with response function experiments to see whether such a relatively simple modelling is likely to explain the dip below a sand pile, as suggested initially by Savage [46]. Indeed from a finite element calculation of a conical pile, we obtain a good qualitative agreement with the available experimental data but we fail to obtain really quantitative agreement, as the dip amplitude and its width seem both underestimated by a factor of almost 30% in the central part of the pile. It is not yet clear whether the elasticity model we use is oversimplified since it contains only two parameters which are sensitive to shear, or whether the preparation procedure under avalanches is not accounted for correctly in the context of the 3D sand pile. We note here the interesting suggestion of Jenkins [50] that the upward moving "stoppage" waves produced when the avalanche hits the ground could modify the main compression axis so that its direction could be further away from the vertical. This effect would indeed enlarge the size of the dip.

The tendency for deposition history or external action like shear or a biaxial compression to modify the constitutive structure of a material was noted in experiments by Oda *et al.* [51] and in numerical simulations by Radjai *et al.* [52] and is at present time still a very open and difficult question. This paper calls for more extensive systematic studies both experimentally and numerically (possibly analytically). The sand pile pressure dip, as interesting as it seems, appears a bit too complex to analyse for the moment. For a better understanding of this crucial issue, this work suggests a systematic use of response function techniques —stress responses as here, as well as displacement responses as in [53–55]— so as to extract several effective constitutive parameters of the material along a given stress-strain history. This is a promising systematic approach, and a possible alternative to sound propagation techniques, which can precisely identify internal structural changes due to external action on a granular material [34]. This is the scope of ongoing projects in our laboratories.

We thank C. Goldenberg, I. Goldhirsch, J. Jenkins, J. Lanuza, S. Luding and J. Snoeijer for fruitful discussions. The work of RPB was supported by NSF grants DMR-0137119 and DMS-0204677.

References

1. For a broad perspective on granular materials, see the focus issue on the physics of granular media of C. R. Acad. Sci. Phys. **3**, 129-245 (2002); the focus issue on granular materials of Chaos **9**, 509-696 (1999); *Physics of Dry Granular Media*, H.J. Herrmann, J.-P. Hovi, S. Luding (Editors), NATO ASI Ser., Vol. **25** (Kluwer, Amsterdam, 1997); R.P. Behringer, J.T. Jenkins (Editors), *Powders and Grains 97* (Balkema, 1997); H.M. Jaeger, S.R. Nagel, R.P. Behringer, Rev. Mod. Phys. **68**, 1259 (1996).
2. J. Šmíd, J. Novosad, *Proceedings of the Powtech. Conference 1981*, Ind. Chem. Eng. Symp. **63**, D3V 1 (1981).
3. R. Brockbank, J.M. Huntley, R.C. Ball, J. Phys. II **7**, 1521 (1997).
4. L. Vanel, D.W. Howell, D. Clark, R.P. Behringer, E. Clément, Phys. Rev. E **60**, R5040 (1999).
5. J. Geng, E. Longhi, R.P. Behringer, D.W. Howell, Phys. Rev. E **64**, 060301(R) (2001).
6. K. Liffman, D.Y.C. Chan, B.D. Hughes, Powder Technol. **72**, 255 (1992).
7. S. Luding, Phys. Rev. E **55**, 4720 (1997).
8. H.-G. Matuttis, Granular Matter **1**, 83 (1998).
9. J.-P. Bouchaud, M.E. Cates, P. Claudin, J. Phys. I **5**, 639 (1995).
10. J.P. Wittmer, P. Claudin, M.E. Cates, J.-P. Bouchaud, Nature, **382**, 336 (1996).
11. J.P. Wittmer, M.E. Cates, P. Claudin, J. Phys. I **7**, 39 (1997).
12. P. Claudin, *La physique des tas de sable*, PhD Thesis, Ann. Phys. (Paris) **24**, no. 2, 1 (1999).
13. L. Vanel, P. Claudin, J.-P. Bouchaud, M.E. Cates, E. Clément, J.P. Wittmer, Phys. Rev. Lett. **84**, 1439 (2000).
14. M.E. Cates, J.P. Wittmer, J.-P. Bouchaud, P. Claudin, Phys. Rev. Lett. **81**, 1841 (1998); Philos. Trans. R. Soc. London, Ser. A **356**, 2535 (1998); Chaos **9**, 511 (1999).
15. J.-P. Bouchaud, P. Claudin, D. Levine, M. Otto, Eur. Phys. J. E **4**, 451 (2001); J.E.S. Socolar, D.G. Schaeffer, P. Claudin, Eur. Phys. J. E **7**, 353 (2002) and **8**, 453(E) (2002); Y. Roichman, D. Levine, I. Yavneh, Phys. Rev. E **70**, 061301 (2004).
16. R. Blumenfeld, Phys. Rev. Lett. **93**, 108301 (2004).
17. D.M. Wood, *Soil Behaviour and Critical State Soil Mechanics* (Cambridge University Press, Cambridge, 1990).
18. H. Makse, N. Gland, D.L. Johnson, L.M. Schwartz, Phys. Rev. Lett. **83**, 50705073 (1999).
19. P.-G. de Gennes, Physica A **261**, 267 (1998); Rev. Mod. Phys. **71**, S374 (1999).
20. M. da Silva, J. Rajchenbach, Nature **406**, 708 (2000).
21. G. Reydellet, E. Clément, Phys. Rev. Lett. **86**, 3308 (2001)
22. D. Serero, G. Reydellet, P. Claudin, E. Clément, D. Levine, Eur. Phys. J. E **6**, 169 (2001).
23. J. Geng, D. Howell, E. Longhi, R.P. Behringer, G. Reydellet, L. Vanel, E. Clément, S. Luding, Phys. Rev. Lett. **87**, 035506 (2001).
24. N.W. Mueggenburg, H.M. Jaeger, S.R. Nagel, Phys. Rev. E **66**, 031304 (2002).
25. J. Geng, G. Reydellet, E. Clément, R.P. Behringer, Physica D **182**, 274 (2003).
26. M.J. Spannuth, N.W. Mueggenburg, H.M. Jaeger, S.R. Nagel, `cond-mat/0308580`.
27. C. Eloy, E. Clément, J. Phys. I **7**, 1541 (1997).
28. J.-J. Moreau, in the proceedings of the *Colloque Physique et Mécanique des Matériaux Granulaires, Champs-sur-Marne (France)* (Laboratoire des Ponts et Chaussées, 2000) p. 199.
29. L. Breton, P. Claudin, E. Clément, J.-D. Zucker, Europhys. Lett. **60**, 813 (2002).
30. C. Goldenberg, I. Goldhirsch, Phys. Rev. Lett. **89**, 084302 (2002).
31. C. Goldenberg, I. Goldhirsch, Granular Matter **6**, 87 (2004).
32. R. da Silveira, G. Vidalenc, C. Gay, `cond-mat/0208214`.
33. S. Ostojic, D. Panja, J. Stat. Mech., P01011 (2005); to be published in Europhys. Lett., `cond-mat/0409160`.
34. A.P.F. Atman, P. Brunet, J. Geng, G. Reydellet, G. Combe, P. Claudin, R.P. Behringer, E. Clément, to be published in J. Phys. Condens. Matter, special issue on *Granular Materials*, edited by M. Nicodemi, `cond-mat/0411734`.
35. N. Gland, P. Wang, H.A. Makse, *Numerical study of the stress response of dense granular packings*, preprint (2004).
36. C. Goldenberg, I. Goldhirsch, to be published in Nature (2005).
37. C. Goldenberg, I. Goldhirsch, Eur. Phys. J. E **9**, 245 (2002).
38. M. Otto, J.-P. Bouchaud, P. Claudin, J.E.S. Socolar, Phys. Rev. E **67**, 031302 (2003).
39. D.A. Head, A.V. Tkachenko, T.A. Witten, Eur. Phys. J. E **6**, 99 (2001); see also the comment of J.-N. Roux, Eur. Phys. J. E **7**, 297 (2002).
40. A. Kasahara, H. Nakanishi, `cond-mat/0405169`.
41. S.F. Edwards, D.V. Grinev, Phys. Rev. Lett. **82**, 5397 (1999).
42. A.V. Tkachenko, T.A. Witten, Phys. Rev. E **60**, 687 (1999).
43. R.C. Ball, R. Blumenfeld, Phys. Rev. Lett. **88**, 115505 (2002).
44. C.F. Moukarzel, J. Phys. Condens. Matter **14**, 2379 (2002).
45. J.-N. Roux, Phys. Rev. E **61**, 6802 (2000).
46. S.B. Savage, in *Physics of Dry Granular Media*, edited by H.J. Herrmann, J.P. Hovi, S. Luding, NATO ASI Ser., Vol. **25** (Kluver, Amsterdam, 1998).
47. A.K. Didwania, F. Cantelaube, J.D. Goddard, Proc. R. Soc. London, Ser. A **456**, 2569 (2000).
48. J. Garnier, *Tassement et contraintes. Influence de la rigidité de la fondation et de l'anisotropie du massif*, PhD Thesis, Université de Grenoble (1973).
49. With CAST3M, see `http://www.castem.org:8001`.
50. J. Jenkins, private communication.
51. M. Oda, S. Nemat-Nasser, J. Konishi, Oils Fundat. **25**, 85 (1985).
52. F. Radjai, D. Wolf, M. Jean, J.-J. Moreau, Phys. Rev. Lett. **80**, 61 (1998).
53. E. Kolb, J. Cviklinski, J. Lanuza, P. Claudin, E. Clément, Phys. Rev. E **69**, 031306 (2004).
54. F. Leonforte, A. Tanguy, J.P. Wittmer, J.-L. Barrat, Phys. Rev. B **70**, 014203 (2004).
55. C.F. Moukarzel, H. Pacheco-Martinaez, J.C. Ruiz-Suarez, A.M. Vidales, Granular Matter **6**, 61 (2004).